Soft Matter

Accepted Manuscript

ROYAL SOCIETY OF CHEMISTRY

www.rsc.org/softmatter

Cite this: DOI: 10.1039/c0xx00000x

www.rsc.org/xxxxxx

COMMUNICATION

Hybrid Hydrogel Sheets that Undergo Pre-Programmed Shape Transformations

Zengjiang Wei,[ab] Zheng Jia,[c] Jasmin Athas,[d] Chaoyang Wang,[b] Srinivasa R. Raghavan,[d] Teng Li*[c] and Zhihong Nie*[a]

Received (in XXX, XXX) Xth XXXXXXXXX 2014, Accepted Xth XXXXXXXXX 2014
DOI: 10.1039/b000000x

This communication describes a novel strategy to achieve programmable shape transformation of hybrid hydrogel sheets by modulating both the in-plane and out-of-plane mismatches in mechanical properties. Both our experimental and computational results demonstrate that the shape transformation of hybrid hydrogel sheets show rich features (e.g., rolling direction, axis, chirality, etc.) and versatile tunability (e.g., via various external stimuli, material properties, and pattern geometry, etc.). This work can provide guidance for designing soft materials that are able to undergo more precise and complex shape transformation.

Shape-transforming phenomena are ubiquitous in living things such as plants. For example, the Venus flytrap can open and close the terminal portion of its leaves, and awns of wild oats rearrange into helices upon desiccation. Such phenomena have inspired the synthesis and design of artificial "smart" systems that can sense changes and adjust their shapes in response to the environment, much as in living organisms.[1-6] The tremendous interest in self-shaping materials stems from their wide range of potential applications, ranging from biomedical devices to optoelectronics. Particularly, shape-transforming hydrogels are attractive because of their tunable responsiveness to stimuli such as temperature, humidity, ionic strength variation, pH, electric current, and light.[7-20] These materials have numerous potential applications in soft robotics,[12] as self-healing materials,[21, 22] in drug delivery,[23] as reactors,[24] actuators,[25] and in three-dimensional (3D) cell culture.[26]

The modulation of sheet-like soft materials (e.g., hydrogels) to induce simple bending and twisting has been widely explored since the early report by Hu et al.[27] Bending of gel sheets primarily relies on the inhomogeneity in the volumetric variation (namely, swelling or shrinking) along the sheet thickness direction in response to stimuli. This is frequently achieved by utilizing bilayer or gradient structures along the thickness direction. Programming soft materials to attain complex 3D shape transformations was not explored until recently. Commonly-used strategies usually involve the multi-step folding of isotropic, stimuli-responsive polymer bilayers to fabricate complex 3D structures like pyramidal cones, multi-arm stars and tubular constructs.[5, 8, 16, 19, 28-32] These methods are based on a hinge-like mechanism and are not capable of creating complex structures with well-defined curvatures.[28] Recently, themodulation of local in-plane stress (without differential volume change along thickness) within sheets has been proven to be a powerful methodology of programming the formation of highly complex shapes.[17, 33-35] These structures are not attainable by conventional approaches based on bilayer or gradient structures. However, relatively small differentiation in in-plane stresses results in limited driving forces to induce shape transformation at large amplitudes. Our hypothesis is that the combination of two strategies, i.e., internal stress modulation and bilayer structure (Figure 1a), would be sufficient to create unique shape-transforming hydrogels that would be otherwise impossible to create using each strategy individually. In this case, the bilayer morphology of the hydrogel provides a sufficiently large driving force to transform as-made 2D hydrogel sheets into 3D, while the compositional patterns enable small-scale modulation of internal stress, which in turn renders programmable tunability of the shape transformation.

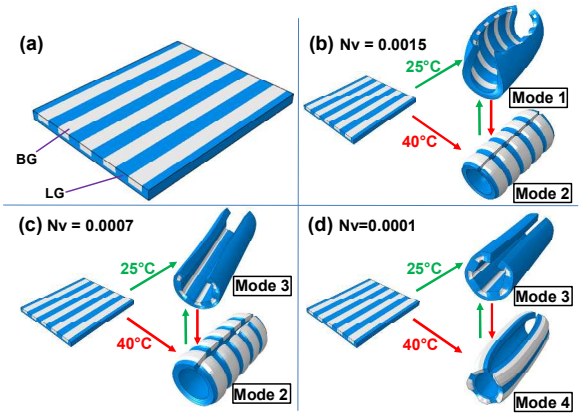

[a] *Z. Wei, J. Athas, Prof. Dr. Z. Nie, Department of Chemistry and Biochemistry, University of Maryland, College Park, MD 20742, USA. Email: znie@umd.edu*
[b] *Z. Wei, Prof. Dr. C Wang, Research Institute of Materials Science, South China University of Technology, Guangzhou 510640, China.*
[c] *Z Jia, Prof. Dr. T Li, Department of Mechanical Engineering, university of Maryland, College Park, MD 20742, USA. Email: LiT@umd.edu*
[d] *Prof. S. R. Raghavan, Department of Chemical and Biomolecular Engineering, University of Maryland, College Park, MD 20742-2111, USA.*

Figure 1. Shape transformations predicted by FEM. (a) Schematic of an as-made bilayer hybrid hydrogel sheet. The blue colour represents the laponite-crosslinked gels (LGs), while the white colour indicates the N,N'-methylene-bis-acrylamide (BIS)-crosslinked gels (BGs). (b-d) Modelling of shape transformation of hybrid hydrogel sheets with a normalized nominal density of polymer chains of BG of Nv =0.0015 (b), 0,0007 (c) and 0.0001 (d). Here N is the nominal density of polymer chains of BG and v is the volume of one water molecule. The resulting shape of hybrid hydrogel sheets submerged in 25°C or 40°C water can be categorized into four modes (denoted as Modes 1, 2, 3 and 4), based on the rolling direction and orientation of the rolling axis.

Without an external mechanical load or geometric constraints, a homogeneous hydrogel network equilibrates with the surrounding solvent by a homogenous and isotropic deformation. Such free swelling can be analytically studied using a thermodynamic framework. However, free swelling of hydrogels rarely occurs in nature. In real scenarios, an anisotropic or inhomogeneous state of deformation occurs in response to an external mechanical load or geometric constraint. To elucidate such inhomogeneous deformation, finite element modeling (FEM) has been implemented recently to study hydrogel deformation under various stimuli and constraints.[36]

Herein, we report the FEM-assisted design of 2D hydrogel sheets with programmable capability to undergo specific shape transformations. The hybrid hydrogel sheets fabricated by multi-step photolithography comprise laponite-crosslinked gels (LGs) and N,N'-methylene-bis-acrylamide (BIS)-crosslinked gels (BGs) (see details of fabrication in SI).[37] The LGs are made from poly(*N*-isopropyl acrylamide) (PNIPAm) cross-linked using nanoparticles of a synthetic clay called laponite.[38] The crosslinking of PNIPAm by laponite proceeds by a free-radical polymerization, while the bonds between laponite and PNIPAm chains are suggested to be non-covalent (polar or ionic).[39-43] The BGs are PNIPAm gels covalently cross-linked by a conventional multifucntional crosslinker, BIS (see detailed recipes in SI). The PNIPAm gel shows a Lower Critical Solution Temperature (LCST) of ~32°C, above which it dehydrates and shrinks. The LGs and BGs show significant difference in elastic modulus and volumetric change in response to external stimuli (e.g., temperature, salt, or solvent).[44, 45] The LGs are softer and swell/shrink more than the BGs. The planar hydrogel sheets comprise two layers: the top layer consists of alternating slender strips of LGs and BGs, and the bottom layer is pure LG (Figure 1a). These hybrid hydrogel sheets undergo a unique shape transformation that is beyond the capability of conventional strategies. We demonstrate that the hybrid hydrogel sheets transform between left-handed and right-handed helices, between tubes with top or bottom sheet surface selectively hidden inside, or between tubular states with different rolling axes in both experiments and simulations. Our study provides a mechanistic understanding on the parameters that govern these shape transformations. We are thus able to offer guidelines to further explore the opportunities afforded by our design strategy.

We started with continuum modeling to investigate the shape transformation of the hybrid hydrogel sheets (Figure 1b-d). In all simulations, the BG strips are perpendicular to the long axis of the hydrogel sheet (Figure 1a). The material properties of the BG and LG are characterized by the nominal density of polymer chains and the enthalpy of mixing. Here, the nominal density of polymer chains describes the number of polymer chains divided by the volume of dry polymer, and the enthalpy of mixing is a measure of the strength of pairwise interactions between polymers and solvent (see details in SI). Our simulations suggest that these two parameters play a critical role in the shape transformation of the hybrid hydrogel sheets. Variation in nominal density of polymer chains or enthalpy of mixing may significantly affect the response (e.g. volume change, etc.) of LG and BG to external stimuli, thus resulting in different morphologies of hybrid hydrogel sheets (Figure 1b-d).

To demonstrate different possible morphologies, we studied hybrid hydrogel sheets with three representative nominal densities of polymer chains in the BG while all other material properties of BGs and LGs are taken to be the same in these three cases (listed in Table S1). Figure 1b illustrates shape transformation of hybrid hydrogel sheets with Nv=0.0015, where N is the nominal density of polymer chains of BG and v represents the volume of one water molecule. Nv is normalized nominal density of polymer chains and is defined as a dimensionless measurement of the polymer chain density. Submerged in pure water at 25°C, LG absorbs more water and hence swells more than BG does, resulting in the rolling up of the 2D hydrogel sheet into a tubular structure with the BG strips hidden inside the tube (denoted as Mode 1). When the water temperature is switched to 40°C, beyond the LCST of the constituent PNIPAm gels, both LG and BG dehydrate and shrink in volume, with the LG shrinking more than the BG. As a result, the tubular hybrid hydrogel sheet in Mode 1 first opens up and flattens, then further rolls into a tubular structure with the BG strips exposed outside (denoted as Mode 2). Moreover, the shape transition between Mode 1 and Mode 2 is fully reversible and repeatable. The rolling direction (so that BG strips are exposed outside or hidden inside) is mainly determined by the difference between the volumetric swelling of BG and LG, $\Delta v = \Delta v_{BG} - \Delta v_{LG}$, where Δv_{BG} and Δv_{LG} can, in principle, be fully specified by the material properties of PNIPAm gels and the solvent environment. Negative Δv results in morphologies with the BG strips hidden inside, while positive Δv renders morphologies with the BG strips exposed outside. Besides the rolling direction, the final shape of a hybrid hydrogel sheet is also characterized by the rolling axis, which is perpendicular to the BG strips in both Mode 1 and Mode 2.

Shape transformation of hybrid hydrogel sheets with Nv= 0.0007 of BG is shown in Figure 1c. While submerging the sheet into 40°C water results in a tubular structure with BG strips exposed outside and a rolling axis perpendicular to BG strips (i.e., Mode 2 as in Figure 1b), decreasing water temperature to 25°C first leads to the flattening of the tubular structure in Mode 2, followed by further rolling about an axis parallel to the BG strips into another tubular structure with BG strips hidden inside (denoted as Mode 3). The transition between Mode 2 and Mode 3 is also fully reversible and repeatable. When the normalized nominal density of polymer chains of BG is taken to be 0.0001 (Figure 1d), the hybrid hydrogel sheet rolls up along an axis parallel to the BG strips into a tubular structure with BG strips hidden inside when submerged in 25°C water (i.e., Mode 3 as in Figure 1c), but with BG strips exposed outside when submerged in 40°C water (denoted as Mode 4). The transition between Mode 3 and Mode 4 here is also fully reversible and repeatable. Characteristics of the abovementioned four modes of 3D shape

transformation from the as-made 2D hybrid hydrogel sheets are summarized in Table S2. The modeling study shown in Figure 1 indicates that the change of nominal density of polymer chains of BG can lead to the switching of rolling axis of the hybrid hydrogel sheets. In addition, the enthalpy of mixing and geometry of BG/LG strips may also have influence on the rolling axis, which requires further systematic numerical studies beyond the scope of this paper and will be presented elsewhere.

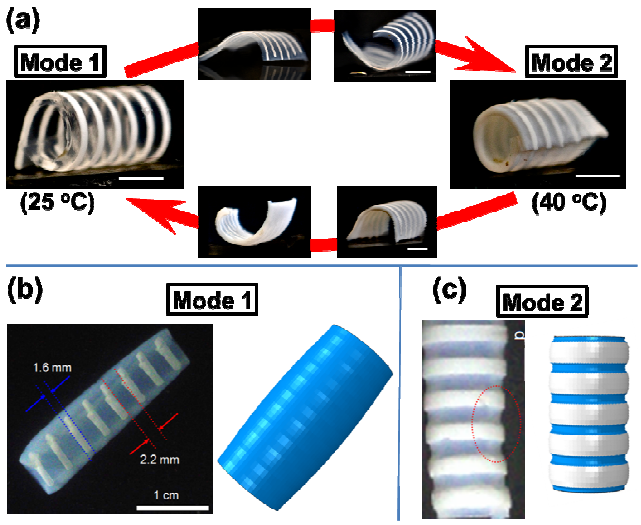

Figure 2. Experimental demonstration of the shape transformation of hybrid hydrogel sheets. (a) Reversible and repeatable transition between Modes 1 and 2, as predicted by simulations. Excellent agreement is seen between the shapes predicted by simulation and those observed experimentally, including in fine details such as: (b) overall fusiform shape in Mode 1; (c) surface undulation morphology in Mode 2. The scale bars are 1 cm.

Instructed by the findings from simulations, we have explored the shape transformation of hybrid hydrogel sheets with designed LG/BG strips. The sheets were fabricated as described in the SI. The shape transformation was triggered by placing the sheet in water at controlled temperatures. We started with hybrid hydrogels with low crosslinking density of BGs (C_{BIS} < 5 mol%). In this case, the stiffness of BGs is comparable to that of LGs. The as-fabricated sheets remained flat on the substrate at room temperature (25°C). When the sheets were immersed in water at 25°C, the LG portions expand more than the BG portions. To accommodate the volume mismatch, the hybrid BG/LG sheets bent towards the BG-strip (top) side about an axis perpendicular to the BG strips, thus leading to the formation of a tubular structure with the BG strips hidden in the interior of the tube (left panel in Figure 2a), as predicted by Mode 1 in the simulations (Figure 1b). When the resulting tubular structure was moved to water having an elevated temperature of 40°C, both the LG and BG portions shrunk and expelled water, with the LGs shrinking more than the BGs. During this process, the tubes first opened up and became flat, and then continuously bent towards the all-LG side, leading to another tubular structure with the BG strips exposed outside (right panel in Figure 2a), as predicted by Mode 2 in the simulations (Figure 1b). We thus see a good agreement between the simulation results and the experimental observations, including in the fine features such as the overall fusiform shape with BG strips wrapped inside in Mode 1 (Figure 2b) and the surface undulation morphology with BGs at peaks and LGs at troughs in Mode 2 (Figure 2c). It is worth noting that the formation of the fusiform shape in Mode 1 results from the bending of sheets along two competing axes as aforementioned: the axis parallel to and that perpendicular to the BG strips. In Mode 1, the bending along the rolling axis normal to the BG strips dominates the deformation of the hybrid hydrogel sheet; but the sheet also tends to roll up along axis parallel to the BG strips, especially at its four free corners (Figure 1b). This combined deformation led to the overall fusiform shape, which proves the existence of the two rolling axes predicted by simulations. Further placement of the tubular hydrogel sheet in Mode 2 into water at 25°C made the sheets recover its original tubular structure in Mode 1 (see both experimental and computational time-dependent transformation in SI). This indicates that the entire shape-transformation is reversible and repeatable. Shape transformations of the hybrid hydrogel sheets can also be achieved by tuning the ionic strength of water or the composition of solvents (e.g., the addition of ethanol, see details in SI). Both simulations and experiments suggest that, the differential volume change in a hydrogel bilayer induces strong and localized internal stresses and determines the rolling direction of the hydrogel sheets, while the asymmetric spatial arrangement of the gel strips serves as the geometric origin of its preferential rolling axis.

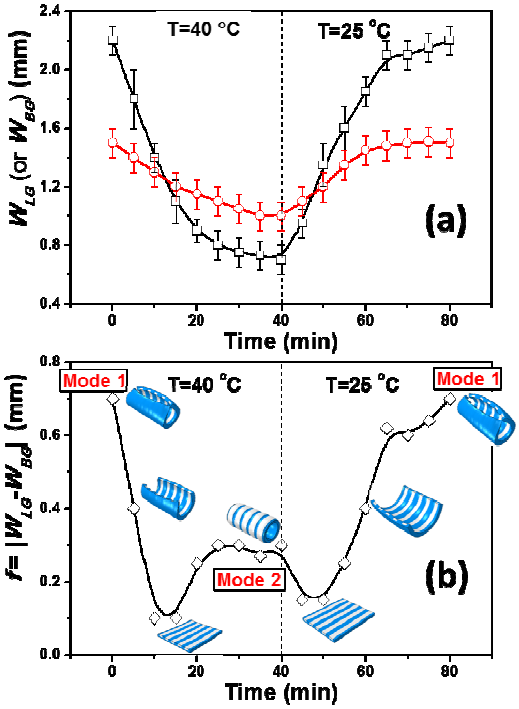

Figure 3. (a) Variation in the BG strip width W_{BG} (red) and LG strip width W_{LG} (dark), and (b) the difference between W_{LG} and W_{BG} of the hybrid hydrogel sheet, as a function of time after a tubular hydrogel sheet in Mode 1 is first immersed in 40°C water and then in 25°C water. The data points are obtained by measuring the dimensions of hydrogel sheets. Computational

images in (b) show the reversible transition from Mode 1 to Mode 2 and back to Mode 1.

To quantitatively understand the shape transformation mechanism, we examined the variation in the width of the BG (W_{BG}) and LG (W_{LG}) strips during shape transformation as a function of time after a tubular hydrogel sheet in Mode 1 was first immersed in 40°C water and then in 25°C water (Figure 3, Figure S6). In 40°C water, both LG and BG shrank, but W_{LG} decreased faster than W_{BG}, as indicated by the steeper slope of the black curve in Figure 3a. Meanwhile, the tubular sheet first unfolded and became flat, and then bent further in the opposite direction to form another tubular structure in Mode 2 (Figure 3b) in ~ 40 min. When this Mode 2 tubular structure was then immersed in 25°C water, both BG and LG swelled, but W_{LG} increased faster than W_{BG}. While swelling, the Mode 2 tubular structure flattened first and then bent further to recover into a tubular structure in Mode 1 in ~ 40 min. This clearly demonstrates the reversible transition between different shapes. The plot of $f = W_{LG}–W_{BG}$ as a function of time (Figure 3b) reveals that tubular structures were formed at peak values of f, while the sheet was flat when f is at its minima.

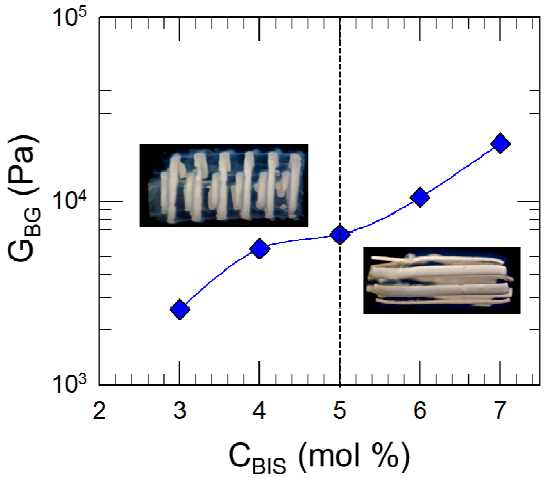

Figure 4. The elastic modulus in shear of the BG, G_{BG} as a function of the concentration of BIS crosslinker. The elastic modulus of the LG is constant (G_{LG} ~425 Pa). Corresponding BG/LG hybrid gels attain shapes depending on the relative values of G_{BG} and G_{LG}, as shown by the photographs in the insets.

The simulations demonstrate that the normalized nominal density of polymer chains in BGs strongly affects the shape transformation of the hybrid hydrogel sheets. It is noted that the nominal density of polymer chains N depends on the crosslink density of the hydrogels. Inspired by these simulation findings, we then varied the crosslink densities of the constituent hydrogels and studied the resultant effects on the shape transformation of the hybrid hydrogel sheets. For this, we varied the elastic modulus (under shear) of the BGs (G_{BG}) by varying the concentration of crosslinker (BIS) and hence the crosslinking density of the gels. At the same time, we maintained the elastic modulus of the LGs (G_{LG}) at ~ 425 Pa. Figure 4 shows that as the concentration of BIS, C_{BIS} was increased from 3 to 7 mol%, G_{BG} increased from ~1,000 to ~20,000 Pa. When hybrid hydrogel sheets with various BG/LG stiffness ratios were immersed in 25°C water, we found that there is a threshold value of C_{BIS} (5 mol%), below which the sheets rolled along an axis perpendicular to the BG strips (Mode 1) while above which the sheets rolled along an axis parallel to the BG strips (Mode 3). The competition between two rolling axes can be explained by the following energetics: the free energy of the hydrogels is composed of the energy due to the stretching of the polymeric network (i.e., the elastic energy) and the energy due to the mixing of the gel with the solvent. The elastic energy of the hydrogel sheets scales with the stiffness of the BG and LG strips. As C_{BIS} increases, the BG strips become stiffer. Above a threshold value of BG stiffness, rolling along an axis perpendicular to the BG strips becomes energetically unfavorable, thus gives way to rolling along an axis parallel to the BG strips which results in minimal deformation of the stiffer BG strips. Nonetheless, comprehensive understanding of the competition between rolling axes and its quantitative dependence on the material properties of the BG and LG still requires further systematic investigation.

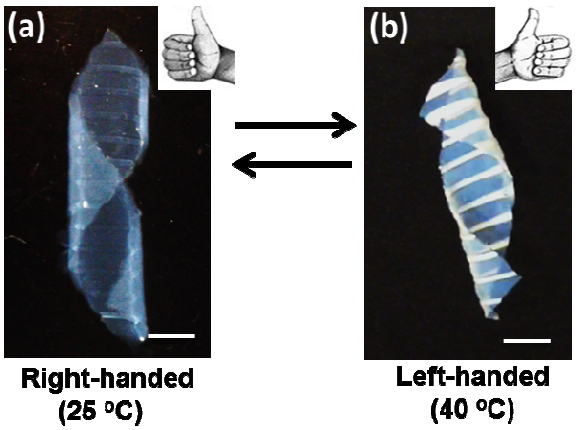

Figure 5. Experimental demonstration of the reversible switching of a hybrid hydrogel sheet from a right-handed helix at 25°C to a left-handed helix at 40°C. Here, the slender strips of BG are at an angle of 45° relative to the long axis of the LG sheet. Scale bars are 1 cm.

Lastly, we demonstrate the reversible switching of hydrogel sheets between states of different chirality. To obtain helical shapes, the hybrid hydrogel sheet was cut along a slant so that the slender strips made an angle of ~45° with respect to the long axis of the sheet (see Figure S3). The immersion of such a hydrogel sheet in 25°C water led to a right-handed helical structure, by bending along the direction parallel to the BG strips (Figure 5a). When the right-handed helix was placed in 40°C water, the helix flattened and then further rolled into a similar helical structure but with opposite chirality, i.e., a left-handed helix (Figure 5b). This transformation was also repeatable and reversible. Such a transition may find potential applications in programming the optical and electronic properties of soft materials and devices.

In summary, we have developed a novel strategy to achieve programmable shape transformation of hybrid hydrogel sheets by modulating both the in-plane and out-of-plane mismatches in mechanical properties. Both our experimental and computational results demonstrate rich features (e.g., rolling direction, axis, chirality, etc.) and versatile tunability (e.g., via various external stimuli, material properties, and pattern geometry, etc.). The general principle emerging from the present study can be applied to design soft materials that are able to undergo more precise and complex shape transformation and thus may find potential applications in drug delivery, actuators, sensors, tissue engineering, and optical and electronic devices.

Supporting Information

The synthetic recipe and experimental details, simulation process, and shape transformation of this hybrid hydrogel response to tmperature and ion concentration. This material is available at http://pubs.rsc.org.

Notes

The authors declare no competing financial interests.

ACKNOWLEDGMENT

ZN acknowledges the financial support from the University of Maryland. TL and ZJ thank the support of NASA (Grant number: NNX12AM02G). ZJ acknowledges a UMD Graduate Dean's Dissertation Fellowship. ZW thanks the support of China Scholarship Council.

REFERENCES:

1. X. M. He, M. Aizenberg, O. Kuksenok, L. D. Zarzar, A. Shastri, A. C. Balazs and J. Aizenberg, *Nature*, 2012, **487**, 214-218.
2. A. W. Feinberg, A. Feigel, S. S. Shevkoplyas, S. Sheehy, G. M. Whitesides and K. K. Parker, *Science*, 2007, **317**, 1366-1370.
3. J. R. Capadona, K. Shanmuganathan, D. J. Tyler, S. J. Rowan and C. Weder, *Science*, 2008, **319**, 1370-1374.
4. P. Fratzl, *J R Soc Interface*, 2007, **4**, 637-642.
5. M. Jamal, N. Bassik, J. H. Cho, C. L. Randall and D. H. Gracias, *Biomaterials*, 2010, **31**, 1683-1690.
6. E. W. H. Jager, O. Inganas and I. Lundstrom, *Science*, 2000, **288**, 2335-2338.
7. J. Kim, J. A. Hanna, R. C. Hayward and C. D. Santangelo, *Soft Matter*, 2012, **8**, 2375-2381.
8. Z. B. Hu, Y. Y. Chen, C. J. Wang, Y. D. Zheng and Y. Li, *Nature*, 1998, **393**, 149-152.
9. H. Inomata, S. Goto, K. Otake and S. Saito, *Langmuir*, 1992, **8**, 687-690.
10. Y. K. Jhon, R. R. Bhat, C. Jeong, O. J. Rojas, I. Szleifer and J. Genzer, *Macromol Rapid Comm*, 2006, **27**, 697-701.
11. D. J. Beebe, J. S. Moore, J. M. Bauer, Q. Yu, R. H. Liu, C. Devadoss and B. H. Jo, *Nature*, 2000, **404**, 588-590.
12. M. Otake, Y. Kagami, M. Inaba and H. Inoue, *Robot Auton Syst*, 2002, **40**, 185-191.
13. F. Peng, G. Z. Li, X. X. Liu, S. Z. Wu and Z. Tong, *J Am Chem Soc*, 2008, **130**, 16166-16167.
14. A. B. Lugao and S. M. Malmonge, *Nucl Instrum Meth B*, 2001, **185**, 37-42.
15. Z. C. Zhu, E. Senses, P. Akcora and S. A. Sukhishvili, *Acs Nano*, 2012, **6**, 3152-3162.
16. Y. Li, Z. B. Hu and Y. Y. Chen, *J Appl Polym Sci*, 1997, **63**, 1173-1178.
17. J. Kim, J. A. Hanna, M. Byun, C. D. Santangelo and R. C. Hayward, *Science*, 2012, **335**, 1201-1205.
18. P. Techawanitchai, M. Ebara, N. Idota, T. A. Asoh, A. Kikuchi and T. Aoyagi, *Soft Matter*, 2012, **8**, 2844-2851.
19. T. S. Shim, S. H. Kim, C. J. Heo, H. C. Jeon and S. M. Yang, *Angew Chem Int Edit*, 2012, **51**, 1420-1423.
20. E. Palleau, D. Morales, M. D. Dickey and O. D. Velev, *Nat Commun*, 2013, **4**.
21. A. Phadke, C. Zhang, B. Arman, C. C. Hsu, R. A. Mashelkar, A. K. Lele, M. J. Tauber, G. Arya and S. Varghese, *P Natl Acad Sci USA*, 2012, **109**, 4383-4388.
22. M. M. Zhang, D. H. Xu, X. Z. Yan, J. Z. Chen, S. Y. Dong, B. Zheng and F. H. Huang, *Angew Chem Int Edit*, 2012, **51**, 7011-7015.
23. J. K. Oh, R. Drumright, D. J. Siegwart and K. Matyjaszewski, *Prog Polym Sci*, 2008, **33**, 448-477.
24. K. G. Lee, J. Hong, K. W. Wang, N. S. Heo, D. H. Kim, S. Y. Lee, S. J. Lee and T. J. Park, *Acs Nano*, 2012, **6**, 6998-7008.
25. G. H. Kwon, Y. Y. Choi, J. Y. Park, D. H. Woo, K. B. Lee, J. H. Kim and S. H. Lee, *Lab Chip*, 2010, **10**, 1604-1610.
26. M. C. Cushing and K. S. Anseth, *Science*, 2007, **316**, 1133-1134.
27. Z. B. Hu, X. M. Zhang and Y. Li, *Science*, 1995, **269**, 525-527.
28. J. Ryu, M. D'Amato, X. D. Cui, K. N. Long, H. J. Qi and M. L. Dunn, *Appl Phys Lett*, 2012, **100**.
29. N. Bassik, G. M. Stern, M. Jamal and D. H. Gracias, *Adv Mater*, 2008, **20**, 4760-+.
30. Y. Liu, J. K. Boyles, J. Genzer and M. D. Dickey, *Soft Matter*, 2012, **8**, 1764-1769.
31. E. Smela, O. Inganas and I. Lundstrom, *Science*, 1995, **268**, 1735-1738.
32. X. B. Zhang, C. L. Pint, M. H. Lee, B. E. Schubert, A. Jamshidi, K. Takei, H. Ko, A. Gillies, R. Bardhan, J. J. Urban, M. Wu, R. Fearing and A. Javey, *Nano Lett*, 2011, **11**, 3239-3244.
33. Z. L. Wu, M. Moshe, J. Greener, H. Therien-Aubin, Z. Nie, E. Sharon and E. Kumacheva, *Nature Communications*, 2013, **4**, 1586.
34. H. Thérien-Aubin, Z. L. Wu, Z. Nie and E. Kumacheva, *J Am Chem Soc*, 2013, **135**, 4834-4839.
35. R. Kempaiah and Z. Nie, *Journal of Materials Chemistry B*, 2014.
36. W. Hong, Z. Liu and Z. Suo, *International Journal of Solids and Structures*, 2009, **46**, 3282-3289.
37. Y. N. Xia and G. M. Whitesides, *Angew Chem Int Edit*, 1998, **37**, 551-575.
38. K. Haraguchi and T. Takehisa, *Adv Mater*, 2002, **14**, 1120-1124.
39. H. Endo, S. Miyazaki, K. Haraguchi and M. Shibayama, *Macromolecules*, 2008, **41**, 5406-5411.
40. K. Haraguchi, H.-J. Li, K. Matsuda, T. Takehisa and E. Elliott, *Macromolecules*, 2005, **38**, 3482-3490.
41. S. Miyazaki, H. Endo, T. Karino, K. Haraguchi and M. Shibayama, *Macromolecules*, 2007, **40**, 4287-4295.
42. M. Shibayama, T. Karino, S. Miyazaki, S. Okabe, T. Takehisa and K. Haraguchi, *Macromolecules*, 2005, **38**, 10772-10781.
43. M. Shibayama, J. Suda, T. Karino, S. Okabe, T. Takehisa and K. Haraguchi, *Macromolecules*, 2004, **37**, 9606-9612.
44. S. J. Banik, N. J. Fernandes, P. C. Thomas and S. R. Raghavan, *Macromolecules*, 2012, **45**, 5712-5717.
45. P. C. Thomas, B. H. Cipriano and S. R. Raghavan, *Soft Matter*, 2011, **7**, 8192-8197.